IEEE Access
Multidisciplinary ⋮ Rapid Review ⋮ Open Access Journal

Received 3 January 2023, accepted 14 January 2023, date of publication 19 January 2023, date of current version 24 January 2023.

Digital Object Identifier 10.1109/ACCESS.2023.3238099

RESEARCH ARTICLE

Error Analysis of Free Space Communication System Using Machine Learning

ALI A. ALTALBE[1,2], MUHAMMAD NASIR KHAN[3,4], AND MUHAMMAD TAHIR[5]

[1]Department of Computer Science, Prince Sattam Bin Abdulaziz University, Al-Kharj 11942, Saudi Arabia
[2]Faculty of Computing and Information Technology, King Abdulaziz University, Jeddah 21589, Saudi Arabia
[3]Department of Electrical Engineering, The University of Lahore, Lahore 54590, Pakistan
[4]Department of Electrical Engineering, GC University Lahore, Lahore 54000, Pakistan
[5]Department of Software Engineering, Sir Syed University of Engineering and Technology, Karachi 75300, Pakistan

Corresponding author: Ali A. Altalbe (a.altalbe@psau.edu.sa)

The authors extend their appreciation to the Deputyship for Research & Innovation, Ministry of Education in Saudi Arabia, for funding this research work through project number (IF2/PSAU/2022/01/22378).

ABSTRACT Free space optical (FSO) communication offers huge bandwidth, license-free spectrum and a more secure channel. PIN diodes are normally used for detection, but avalanche photodiodes (APD) are preferred for detecting high-speed FSO signals in many applications. In the case of APD, the noise distribution is input-dependent Gaussian noise (IDGN) rather than input-independent Gaussian noise (IIGN). We investigate the error analysis using on-off keying (OOK) for various detection approaches. This paper proposes a machine learning approach and compares its performance with soft and hard decisions. Soft values in the case of IDGN and IIGN are derived, and the optimum and sub-optimum detection thresholds are evaluated. The proposed novel ML approach shows better performance gains than the other approaches. It is also demonstrated that the IDGN model should have an optimum detection and achieve a gain of 2.5[dB] and about 1[dB] at $\lambda = 0$[dB] and $\lambda = 10$[dB], respectively. Experimental results are plotted for the FSO channel data, and a model fit curve is plotted using the ML approach.

INDEX TERMS Error analysis, machine learning, optical communications, hard decision, soft decision.

I. INTRODUCTION

The prevalence of smartphone applications has been growing on a large scale over the last decades, and the continuous increase in the number of applicants over the globe is being seen every day. Because of the additional broadband channels, there is a dire requirement for wireless networks with increased capacity [1]. From the 9th financial survey of Cisco [2], it was predicted that data traffic of smartphones would be increased significantly, which requires a huge spectrum and data transmission with high speed. The existing radio frequency (RF) spectrum is insufficient to support the additional broadband channels. There are also other issues with the RF spectrum, including the cost-expensive, unsafe, eavesdropping, and bandwidth constraints [1], [3]. Besides all, RF spectrum also requires an expensive license, and its link is not so prone to attacks making it unsafe and insecure for data transmission [4], [5]. Because of many issues, internet service providers and mobile phone companies plan to opt for a different technology, which offers a huge spectrum, secure link and high-speed data transmissions [6], [7].

The alternate solution is recommended by free space optics (FSO) that exploits the light channel to transfer the data over the wireless link. These light channels include light amplification with stimulated emission of radiation (LASER) and positive-intrinsic-negative (PIN) diodes. FSO is a vital wireless technology which offers numerous advantages and has been demanding for various applications over the past ten years [8]. FSO is fiberless and referred to as wireless optical communication (WOC) and laser communication (Lasercom). FSO is a promising technology that offers many broadband channels with a secure link of end-to-end connection over clear sky conditions. FSO working principle is somehow similar to the optical cable. The difference between the wireless and the fiber cable is that the dedicated link is used in fiber optic cable, while the air is exploited in the case

The associate editor coordinating the review of this manuscript and approving it for publication was Tony Thomas.

TABLE 1. System parameters.

Name	Symbol	Name	Symbol
Visibility [Km]	$\mathcal{V}$	Size distribution	q
Wavelength	ζ	Visibility Reference	ζ_o
APD Gain	G	Attenuation Coefficient	$\mathcal{T}$
Cloud attenuation	C_a	Liquid water content	$\mathcal{L}$
Scintillation index	σ_I^2	Noise Temperature	T
Received irradiance	I	Beckman distribution components	r, d, σ_z^2
Mean of Logarithm of I	$\mu_{\ln I}$	Variance Logarithm of I	$\sigma^2_{\ln I}$
GG scattering parameters	α, β	Modified Bessel function	K_a, Γ
Transmit symbols , bits	$\mathcal{X}, x$	Received symbols, bits	$\mathcal{Y}, y$
Transmit power	P	Channel fading	h
FSO link attenuation parameter	ρ	Efficiency	η
Background irradiance	λ	Gaussian noise random variable	w
APD excess noise factor	F	APD ionization co-efficient	k_{eff}
LLR mapping	Λ	Johnson's noise variance	σ^2_{th}
Planck's constant	h_p	Frequency	ν
Photoelectrons	k	Photoelectrons	$\overline{n}$
Encoder (ML)	f_{θ_T}	Decoder (ML)	h_{θ_R}

of FSO. It is to be noted that the wireless link is preferred in such scenarios where it becomes hard or impossible to dig the roads or the solution is not cost-effective [9], [10]. Table 1 defines the symbols used in the paper.

The amount of data transferred in every communication system is directly proportional to the modulated carrier's bandwidth. The maximum data bandwidth that may be used is up to 20% of the carrier frequency. This is because the carrier optical frequency, which covers visible, infrared, and ultraviolet frequencies, is significantly bigger than the RF on the electromagnetic spectrum [11]. An optical source, specifically a laser (light amplification by stimulated emission of radiation), offers a narrow beam size of order divergence of 0.01–0.1 mrad. Light focused in a small region, giving an FSO link appropriate spatial separation from possible interference. Laser beams function almost independently, allowing limitless degrees of frequency reuse in various situations and making data interception difficult for unintended users. The narrowness of the beam, on the other hand, necessitates more stringent alignment criteria. Congestion in RF wireless communication occurs due to tightly spaced carrier frequencies. To get a small bandwidth of the RF spectrum, you'll have to pay a lot of money and go through several months of document processing by authorized departments. Optical frequencies are currently devoid of all of this. Because there are no licensing charges and no long document processing, it also provides economic operations [12]. FSO installation and its operations are economical due to no need for a license, no trenching, no need to get cost of ways, easy installation etc. However, RF communication is almost double as expensive as FSO and not as competent as FSO. Starting with installation and ending with link alignment, the time it takes for an FSO link to become completely operational might be as little as four hours. The most important prerequisite is constructing an unobstructed line-of-sight (LOS) between the transmitter and receiver. It may also be readily dismantled and re-deployed to a different site.

The promising characteristics of FSO make it particularly appealing for a wide range of applications in access and urban infrastructures. It may easily accompany various technologies, such as wireless connectivity, RF communications, and wired fibre-to-the-X technologies, making the massive frequency band in an optical fibre foundation accessible to target consumers. FSO has been proven acceptable for usage in emerging application areas. Last mile access, i.e., links ranging from 50 metres to a few kilometers (Km), are easily offered on the market, with data speeds ranging from 1 Mb/s to 10 Gb/s. FSO is considered for the backup used to prevent data loss or communication breakdown. In third and fourth-generation networks, FSO can carry IS-95 CDMA data signals from micro and macro cells and act as back-haul traffic between switching centers and base stations. With the increase in online conferencing and other ad-hoc connectivity, a quick and temporary data link is needed. In these cases, FSO deployment is an attractive and viable solution for disaster recovery. Backup and interconnecting different inter and intra-campus transmission links is a prominent application of FSO, and it provides speed in the range of up to several Gbps. FSO is increasingly being utilized in the broadcast business to transfer live signals from HD cameras in remote areas to a central office (CO) due to its competency to support high data rates. Hospitals, the military, satellite communication, light-fidelity, CCTV systems, and universities are some of the other particular uses of FSO.

Unfortunately, severe weather scenarios and atmospheric turbulence significantly affect the FSO system's link, and the transmission is blocked by the attenuation caused by disturbances [11], [12]. The optical light beam is scattered and absorbed because of heavy snow, fog, cloud, dust, smoke and haze, and it causes data loss. While the unfavourable weather condition due to earth and sun heat cause atmospheric turbulence, referred to as scintillation [13]. The optical channel conditions should be broadly computed in poor weather to ensure the strong received signal strength for processing. The authors have addressed many ways to overcome the external atmospheric effects and enhance the optical system performance. In the current research work, new error analysis methods are suggested using the latest machine learning technology. Further error analysis is to be compared with three different techniques: hard decision, soft decision and machine learning.

Although FSO technology has a greater impact than the various available technologies, it experiences several boundaries that interrupt its typical functioning and affect its performance. The crucial FSO systems parameters are of two types: internal parameters and external parameters. Major internal parameters include the link margin, receiver sensitivity, FSO wavelengths, power and beam alignment. The external parameters are the weather conditions (e.g., fog, snow, clouds, dust and haze), scintillation, molecular absorption, and turbulences. Atmospheric attenuation and turbulence (i.e., scintillation) significantly deteriorated the FSO system performance.

A. ATMOSPHERIC ATTENUATION

The phenomena of scattering and absorption cause atmospheric attenuation. If considering the outdoor FSO

communications, the FSO link is mostly affected by atmospheric attenuation and turbulence factors. Selecting the FSO transmission wavelength is more effective (850nm to 1600nm). For most applications, the suggested wavelengths are 850nm and 1550nm. The other reason for selecting these wavelengths is the effect on the retina of the eye [14]. The major components affecting the FSO links include fog, snow, smoke, haze, and dust, and the effect of rain is considered negligible. Various visibility models have been developed, including the Mie theory and the Kruse and Kim [15], [16], [17] models. In many applications, 1550 nm window is selected and is investigated under cumulative effects of weather instabilities and scattering. It was found that the performance of 1550 nm is superior to 850 nm over long and short distances due to less scattering and attenuation in free space [18]. The attenuation models over a particular distance for known visibility are given by;

$$\mathcal{V}_{Km} = \frac{10 \log \mathcal{T}}{\epsilon\zeta} \times \left(\frac{\zeta}{\zeta_o}\right)^{-q}, \tag{1}$$

where $\mathcal{V}_{Km}$ is the visibility in Km, $\epsilon\zeta$, $\mathcal{T}$ denotes the atmospheric attenuation coefficients and ζ in nm represents the wavelength, and ζ_o is the visibility reference (550nm), and q is the size distribution, which the Kruse expresses as;

$$q = 0.585\mathcal{V}^{1/3}, \tag{2}$$

According to [14], q is expressed as,

$$q = \begin{cases} 1.6 \ \text{ if } \mathcal{V} > 50 \text{ Km} \\ 1.3 \text{ if } 6 \text{ Km} < \mathcal{V} < 50 \text{ Km} \\ 0.585 V^{\frac{1}{3}} \text{ if } \mathcal{V} < 6 \text{ Km} \end{cases} \tag{3}$$

It is seen from (5) that attenuation effects are less severe for higher operating wavelengths. Simulation results for the Kim and Kruse models are evaluated and compared using different wavelengths. The attenuation for 850nm is more than for the 1550nm assuming the Kruse and Kim models [16], [17] as shown in Figure 1 and 2. This work aims to investigate FSO link performance under different frequency ranges. The simulation results show that as the visibility decreases, the attenuation increases, which attenuates the received signal power.

Signal attenuation in FSO communication can also be caused by rain and happens when the wavelength size is smaller than the rain droplet size. The connection may be disrupted if it rains heavily. Rain attenuation, however, has little effect when compared to fog [19], [20], [21]. In fog, attenuation occurs due to suspended ice droplets in the air and visibility reduced to less than a Km with 100% relative humidity. Fog intensity is categorized based on the following parameters: temperature, particle size, humidity, water content, etc. However, particle size is considered for the distribution model in fog, such as in Gamma distribution [22], [23], [24]. Particle size is the only parameter to explain the event of fog. It is also evident that high attenuation happens in fog due to the same wavelength and particle size.

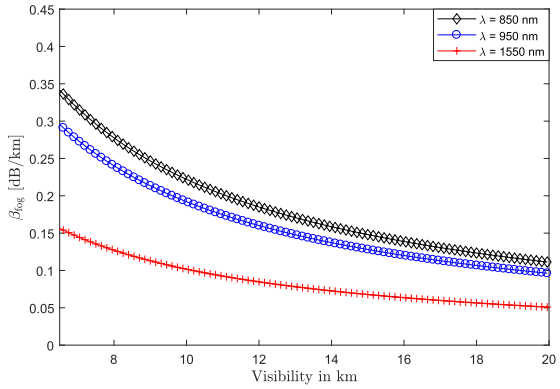

FIGURE 1. Specific attenuation over the visibility.

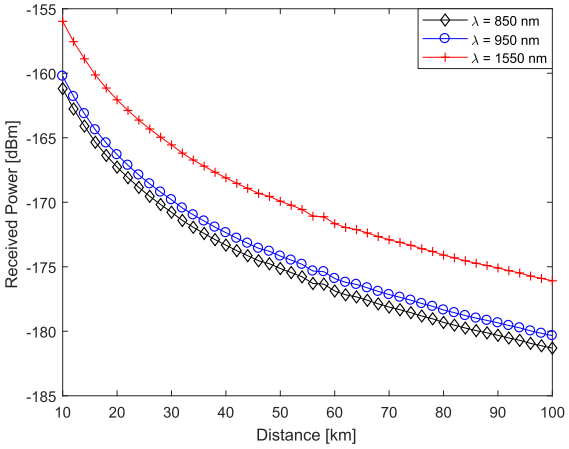

FIGURE 2. Received power over varying channel distance.

In mild fog, the attenuation touches as high as 130 dB/Km and further increases to 480 dB/Km with poor visibility.

Haze is a particular matter which is the combination of dust and smoke in the atmosphere distributed randomly and leads to chemical reactions due to gaseous pollutants. It is sometimes referred to as Mie scattering due to the transmitter wavelength, and almost similar size of haze particles [23], [24], [25]. Visibility is roughly 10 Km but can reduce due to fire and other seasonal occurrences. The optical signal's intensity has deteriorated significantly, and unfavourable weather conditions (e.g., fog, cloud, snow, haze, and dust restrict its range. In [26], [27], [28], and [29], it is explored that the optical links operating at 1550nm experience attenuation of up to 270dB/Km in heavy fog scenarios and is a restricted coverage area of 200 meters.

The beam dispersion, background irradiation, and shadowing effect are optical link performance disruption factors. The efficiency of the FSO system is limited if you measure the bit error rate (BER), signal-to-noise ratio (SNR), periodicity, channel capacity and outage probability. Any undesired items in line-of-sight (LOS) connections disrupt the interaction between the transmitter and receiver [30], [31], [32], [33]. Clouds are referred to as the water droplet collection and the

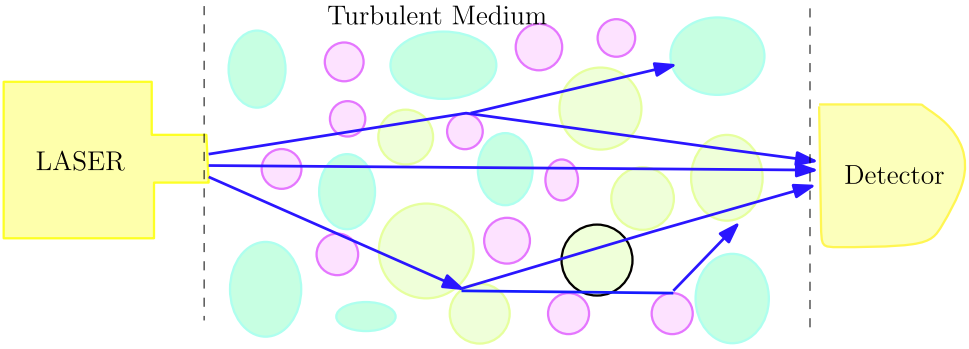

FIGURE 3. Turbulent optical medium.

floating crystal in the air, which degrade the optical channel performance. On passing the optical signal from the clouds, the signal undergoes dispersion, attenuation and absorbance. Similarly, non-selective scattering is one of the main factors affecting the reliability of the optical links. The larger raindrop size and heavy fog cause the light beam to reflect and refract [17], [30], [31], [32].

B. ATMOSPHERIC TURBULENCE IN FSO

The optical link mostly affects atmospheric turbulence, beam pointing loss, and weather attenuation. In addition, there are three crucial factors: airflow velocity fluctuations, uneven scintillation throughout the sphere, and unpredictable wind track. The effect of the atmospheric turbulence distributing the optical signal link gives rise to optical beam deviations. Such optical beam deviation is caused by the atmospheric turbulence brought on by phase shifts of the transmitted optical beams [34], [35], [36]. Various weather scenarios ended up with scintillation, which distorts the optical link significantly. Atmospheric turbulence is a crucial factor that strongly impacts the optical channel, and many useful techniques are addessed to mitigate it [37].

Even under clear sky conditions, clear air turbulence severely affects the FSO system capacity. The heat caused in the atmosphere caused by the sun and wind serves as two factors responsible for inhomogeneities in atmospheric conditions. These inhomogeneities result in irregular variations in air's refractive index, producing air sacs or eddies with diverse sizes and refractive indices. These refractive indexes and propagation track disparities result in arbitrary vacillations across amounts and the received signal phases.

An optical source sends the message wirelessly, i.e., analogue or digital. The FSO signal emphasizes the photodetector positioned at the receiving end, electronically adapted to obtain the input signals. Nevertheless, the influence of atmospheric turbulence on the input message signal has been determined. It is established on the size of the stormy cell and can be abridged as follows:

- The message signal will be bent or distorted on getting the small size of the stormy cell. The variations of the optical signal are observed for different time spans at the receiving end, which ends up over constructive and destructive interference. The authors call this term "scintillation".
- The message signal will be bent on getting the small size of the stormy cell. In such cases, the optical message signals are diverted over the axis on passing through the air cell, which is the scenario of lack of scintillation.

C. CLOUD ATTENUATION

Clouds form when water vapour rises and condenses in the air as water droplets. These water droplets are tiny and light enough to float in the air. However, water droplets can freeze into ice crystals if they appear at a cold temperature due to different cloud heights from the ground. Therefore, there are three main types: high-level, middle-level, and low-level clouds. Those types consist of only ice crystals, mainly ice crystals, and primarily water droplets. Among them, low-level clouds (under 3 Km) affect optical signals the most because of Mie scattering, i.e., the size of a water droplet is much larger than the optical wavelength [21]. They become the main challenging issues for free-space lasercom links. Clouds affect both optical signal power and visibility by reducing their values significantly. Given the visibility in equation 1 and using the Kim model, the cloud attenuation can be expressed by;

$$C_a = \sum_{j=1}^{J} 4.34 \left(\frac{3.91}{\mathcal{V}_j} \left(\frac{\lambda}{550} \right)^{-q_j} \right) \frac{\mathcal{L}_j}{\sin(\theta)}, \tag{4}$$

In this case, the size distribution coefficient based on the scattering particle can be evaluated using the Kim model as;

$$q = \begin{cases} 1.6 & \text{if } \mathcal{V} > 50 \text{ Km} \\ 1.3 & \text{if } 6 \text{ Km} < \mathcal{V} \leq 50 \text{ Km} \\ 0.16V + 0.34 & \text{if } 1 \text{ Km} < \mathcal{V} \leq 6 \text{ Km} \\ V - 0.5 & \text{if } 0.5 \text{ km} < \mathcal{V} \leq 1 \text{ Km} \\ 0 & \text{if } \mathcal{V} \leq 0.5 \text{ Km} \end{cases} \tag{5}$$

The turbulent optical medium is shown in Fig. 3. The scintillation index over the received irradiance I is given

by [6], [8], [22],

$$\sigma_I^2 = \frac{\mathbb{E}\{I^2\}}{[\mathbb{E}\{I\}]^2} - 1, \tag{6}$$

where $\mathbb{E}$ represents the ensemble average operator.

Turbulence can be divided into *weak, moderate and strong*. The irradiance fluctuations' depends on the scintillation strength. According to [6], [11], and [12], the lognormal distribution is commonly used to represent weak scintillation, while the exponential is used to describe strong turbulence [3]. Whereas for moderate scintillation conditions, not much literature is available, while the Beckmann, Gamma-Gamma (GG) and K-distribution are based on heuristic arguments [3]. Authors in [15] modelled the moderate scintillation by a lognormal distribution, whose probability density function (pdf) is expressed as,

$$p^{weak}(I) = \frac{1}{\sqrt{2\pi\sigma_{\ln I}^2 I}} \exp\left[-\frac{(\log(I) - \mu_{\ln I})^2}{2\sigma_{\ln I}^2}\right], \tag{7}$$

where $\mu_{\ln I}$ and $\sigma_{\ln I}^2$ is the mean and variance of the logarithm of I and the natural logarithm by log(.). Authors in [3], use $\mu_{\ln I} = -0.5 \times \sigma_{\ln I}^2$ and $\sigma_{\ln I}^2 = \log(\sigma_I^2 + 1)$. The researchers in [11], suggested the exponential distribution for strong scintillation,

$$p^{strong}(I) = \frac{1}{\mu_I} \exp\left(-\frac{I}{\mu_I}\right), \tag{8}$$

where $\sigma_{\ln I}^2 \triangleq \langle(\ln I - \mu_{\ln I})^2\rangle$ denotes the log-irradiance variance, $\mu_{\ln I} \triangleq \langle \ln I\rangle$ and $\mu_I \triangleq \langle I\rangle$. The Beckmann distribution is [21], [22],

$$\begin{aligned} p^{Beck}(I) &= \frac{(1+r)\exp(-r)}{\sqrt{2\pi\sigma_z^2}} \int_0^\infty I_0\left\{2\left[\frac{(1+r)rI}{z}\right]^{1/2}\right\} \\ &\quad \times \exp\left\{-\frac{(1+r)I}{z} - \frac{[\ln z + (1/2)\sigma_z^2]^2}{2\sigma_z^2}\right\}\frac{dz}{z^2} \quad I > 0, \end{aligned} \tag{9}$$

where the distribution components are denoted by r, z and σ_z^2 and the modified Bessel function is I_0. The GG distribution is given by [21], [22],

$$\begin{aligned} p^{GG}(I) &= \int_0^\infty p_y(I|x)p_x(x)dx \\ &= \frac{2(\alpha\beta)^{(\alpha+\beta)/2}}{\Gamma(\alpha)\Gamma(\beta)} I^{(\alpha+\beta)/2-1} K_{\alpha-\beta}(2[\alpha\beta I]^{1/2}) \quad I > 0, \end{aligned} \tag{10}$$

where α and β denotes distribution scattering parameters (weather dependent) and the modified Bessel function of the second kind and order α by $K_\alpha(.)$ and Γ is the Gamma function. In [22], α and β is evaluated. The K-distribution is [22],

$$p^K(I) = \frac{2\alpha}{\Gamma(\alpha)}(\alpha I)^{(\alpha-1)/2} K_{\alpha-1}(2[\alpha I]^{1/2}) \quad I > 0, \alpha > 0, \tag{11}$$

II. MITIGATION TECHNIQUES

To mitigate the challenges of the FSO system, various techniques, e.g., pointing, acquisition and tracking (PAT) [37], exploiting diversity combining [38], and hybrid radio/optical systems [30], are developed and investigated to get better link availability. Other types of optical signal blockage on a temporary base (e.g., drones, birds, industrial wastes, UAVs, skyscraper wobbles and uprooted trees etc.) cause obstructions in LOS connectivity. However, these communal deteriorations can be efficiently undertaken by applying multi input multi output (MIMO) technology. Exploiting the MIMO-FSO technique, such temporary blockage of the signal on the transmitting and receiving side can be washed out either partially or completely. Such techniques are strongly utilized along with powerful laser sources to mitigate atmospheric turbulence and maintain data reliability. But keep in mind that the more powerful laser sources are not good for retina eyes if the laser beam's values are above the threshold. Therefore, before operating the laser beam, one should consider the safety requirements, which are of utmost importance in OWC.

Besides, managing the laser intensity during the release in OWC is critical. Adaptive controlled approaches are also suggested to enhance the OWC capacity and mitigate the scintillation. Under clear sky conditions, the optical beam propagates uninterrupted, proving that small signal strength is enough under such weather conditions. However, sufficient signal strength is essential to attain suitable levels of throughput, BER and quality of service (QoS). The differences in temperature, region, wind speed, altitude, air pressure, air humidity, etc., seriously influence the FSO lines' temporal variability.

The PAT method is considered an effective and crucial technique for the steadiness and consistency of optical beams [21]. As per [30], a satellite signal requires only 1-10 μrad of pointing precision for attaining a data rate of 10Gbps. Alternatively, wavefront deviations can be distinct as optical phase oscillations transported on by air turbulences while broadcasting through a wireless medium. These wavefront alterations are typically measured using a coupled camera or front wave sensor, although deformable mirrors (DMs) are used to rectify these errors. A laser power source discharges the Gaussian beam from a remote location, and it becomes aberrated when it moves across space. The optical lenses gather all the incoming beams, separating them into light beams of replicated beams and broadcasting pulses. The replicated rays attack the charged coupled camera device (CCCD) while broadcasting signals across the photodetector. The digital signal processors (DSP) drive the DM to detect deviations accurately by generating the essential signal

dependent on CCCD outputs. By eliminating phase errors and integrating cutting-edge optics into FSO communication, the worth and reliability of the system upsurge [38].

However, numerous researchers propose promising mitigation techniques to resolve the technical encounters that might occur in FSO communication systems. A closed-form mathematical expression is developed in [39] for neutralizing the scintillation in FSO links, but it is not exploited to attain numerous objectives; .g., it does not speak about how to lengthen the transmission range. Incorporating an adaptive advantage element to accurate phase deviations by air disorder is wanted. The optical coupler and polarizer can enhance the handling difficulty, and it is not acclaimed for low-latency optical communication systems. Current expansions for OFDM-based radio over FSO (RoFSO) have established convincing connection distance upsurge beneath numerous atmospheric environments [37], [38], [39]. For 5G telecommunications in approaching years, the drawbacks of multiplexing to raise data rate and engaging low order modulation to advance reliability include lengthier processing times and lesser data rates. Additionally, OFDM-based communication has a concern with peak-to-average power deviation.

The authors in [40] projected a network management model to enhance system capacity and mitigate the scintillation effects. But because of some challenges, they could not attain a better BER and data rate. To minimize the FSO turbulence effects, spatial diversity combining techniques is developed using the BPSK mapping technique [33]. On the contrary, using this technique originates other challenges, e.g., the system becomes complex, and the throughput is limited. The authors in [37] developed a coded-orthogonal frequency division multiple access (C-OFDM) technique and presented scintillation in optical links to improve this issue. This technique enhances the system performance with better BER and moderate computational complexity. However, the technique is very simple and easy to develop as well. In particular, it can be further combined with the optimization methods for tackling other issues, e.g., weather attenuations etc., of OWC systems.

Several optimization methods have previously been developed to improve system performance under various conditions and constraints. By exploiting the MIMO networks, a suitable optimization system was developed to enhance the OWC system performance [35]. In this type, both issues, e.g., pointing error and moderate scintillation, were considered. The other constraints, like optical power and divergence angle, were also optimized over a fixed BER. But the closed-form expressions were not derived for such a system. Similarly, in [36], authors improve the optical system's performance by considering the Log-normal and Gamma-Gamma distributions with the assumptions of pointing error, beam width, pointing error variance, and detector size. Some methods in [37], [38], [39], and [40] consider the intensity modulation/direct direction (IM/DD), the misalignment paradigm, and the closed-form expression of the BER assuming moderate scintillation and pointing error was derived [37], [41], [42], [43].

III. OPTICAL TRANSMISSION SYSTEM

An optical communication system block diagram is presented in Fig. 4. The information bits $x \in (0, 1)$ encoded using any encoder, and the resultant bits are propagated through the channel using the ON-OFF keying (OOK), where the light pulse presence transmits bit "1" and the absence bit "0". The assumptions are moderate scintillation, background irradiance and the IDGN. The photodetector receives the optical beam on the receiving side, which translates the light beam into an electrical signal. The signal is then decoded and de-mapped to retrieve the estimated transmitted information. The main blocks of the transmission include the sender, medium and sink. The sender combines the coding (i.e., ENC), the mapper (MAP), light diode, and optics, while the sink is known as the light detector (PIN/APD), de-mapper (D-MAP) and coder. An elaboration on each part is compromising, and the presented research focuses on the main problem of error analysis; via hard decision, soft decision, and machine learning.

A. FSO CHANNEL MODEL

A light signal is propagated through the turbulent media, which affects signal strength. Optical signal transmission can be done either using non-coherent (i.e., intensity modulation with direct detection (IM/DD)) or coherent (heterodyning) [2]. To make the system simple, IM/DD is preferred. IM/DD is popular because of its low complexity and simple receiver design. In the present research work, authors present two signal models, i.e., input-dependent and independent Gaussian noise models. Numerous research [26], [44], [45] have shown that the received optical signal intensity is affected by various components (scintillation, weather attenuation and other light sources, e.g., sun, stars and other artificial light sources). Authors have introduced a generalized system model to incorporate the effects of all natural and artificial light sources.

Let's consider P denotes the optical transmit power, and the transmitted symbols are denoted by x exploiting the simple OOK mapping scheme. The received signal[1] y for the IDGN model is [30],

$$y = (\lambda + \rho g P h x) + \sqrt{(\rho g P h x + \lambda + \sigma_{th}^2)} w \qquad (12)$$

where h denotes the optical link fading, the background irradiance by λ, σ_{th}^2 represents Johnson's noise variance, $w \sim \mathcal{N}(0, 1)$, ρ is the FSO link attenuation parameter and the optical link losses are denoted by g.

Authors in [21] and [45] have neglected the contribution of λ considering that λ does not contribute to the input-output optical link MI and the signal model is then represented by (13). The system model given in (12) and (13) are more general signal models with all the counterparts

[1] ignoring the constant scaling co-efficient (i.e., η) for simplicity

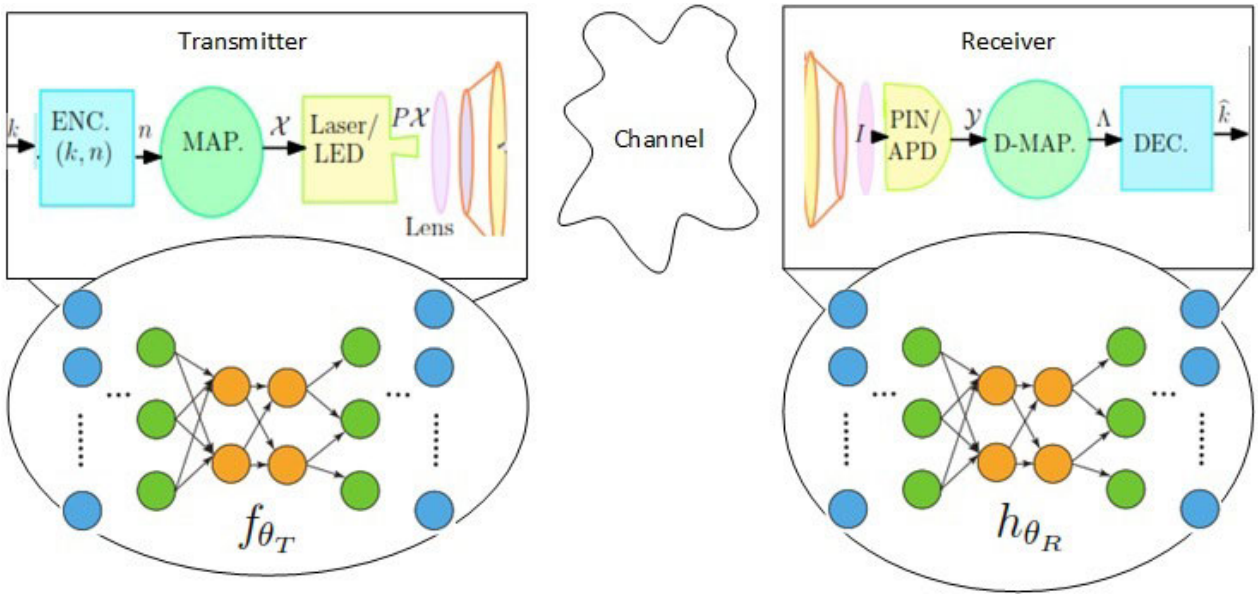

FIGURE 4. Free Space Optical Communication System.

taken into account. According to [46] and [47], the simplified received signal model by neglecting the contribution of input dependent is given by (13). So the system models given by (12) and (13) represent the input-dependent Gaussian noise (IDGN) models while (13) denotes the input-independent Gaussian noise model (IIGN). Equation (12) is then further simplified to,

$$y = \rho g P h x + \sqrt{(\rho g P h x + \lambda + \sigma_{th}^2)} w \tag{13}$$

The implication of (12) and (13) are based on the assumptions of IDGN channels. Considering the assumption of $\lambda + \sigma_{th}^2 \gg \rho g P h x$, (13) can be further simplified for the IIGN model,

$$y = \rho g P h x + \sqrt{(\lambda + \sigma_{th}^2)} w \tag{14}$$

No doubt, the misalignment and window attenuation are optical signal deterioration factors. A LOS and perfect alignment is considered in the proposed study, and it is a reasonable assumption. However, scintillation and weather attenuation factors play an important role in attenuating the optical received signal [2], [12] and therefore, the focus of the proposed study is on turbulence and weather attenuation.

B. INPUT INDEPENDENT SIGNAL MODEL APPROXIMATION

Researchers in [26] and [27] have derived the channel model. Considering the assumptions in [26], we assume the Gaussian approximation of [27]. Then the absorption of the average number of photons at the receiver for a given power is,

$$\bar{n} = \left(\frac{\eta}{h_p \nu}\right) P \tag{15}$$

where the frequency is ν, Planck's constant is h_p. As per [27], we can utilize the Poisson distributed random variable n whose pdf is $p(n) = (\bar{n}^n/n!)\exp(-\bar{n})$. The channel pdf $p(k|\bar{n})$ over output photoelectrons k if McIntyre-Conradi gives the $\bar{n}$ photons are absorbed (MC) [26]. The MC derived the pdf is assumed to be the exact mathematical analysis and has been approximated [27]. In [29], authors assumed the IDGN model, which is the exact approximation of [26] and is given by,

$$p_{IDGN}(k) = \frac{1}{\sqrt{2\pi \bar{n} G^2 F}} \exp\left(\frac{-(k - \bar{n}G)^2}{2\bar{n}G^2F}\right) \tag{16}$$

where $F = k_{eff} G + (2 - 1/G)(1 - k_{eff})$ is the excess noise factor, G is the average APD gain and k_{eff} is the ionisation ratio constant. The pdf of the Webb and Gaussian models over several given photoelectrons are evaluated as shown in Fig. 5, which gives an agreement over an average number of photoelectrons.

Further to our signal model, we assume the bit "1" to be $\bar{n}_1$ (i.e., $\bar{n}_1 = \lambda + Ph$) and bit "0" be $\bar{n}_0$ (i.e., $\bar{n}_0 = \lambda$). We adopt the LN distribution for intensity fluctuations assuming the moderate turbulence conditions [30], whose pdf is given by,

$$p_h(h) = \frac{1}{\sqrt{2\pi\sigma_{lnh}^2} h} \exp\left[-\frac{(\log h - \mu_{lnh})^2}{2\sigma_{lnh}^2}\right] \tag{17}$$

where μ_{lnh} and σ_{lnh}^2 denotes the mean and variance of the logarithm of h. Further, $E[h] = 1$ to keep the average received optical power constant. The mean, $\mu_{lnh} = -\frac{1}{2}\sigma_{lnh}^2$ and $\sigma_{lnh}^2 = \log(1 + \sigma_I^2)$, where σ_I^2 [32]. The physical parameters of the APD are related to the statistical parameters of the IDGN model as $\mu_x = \bar{n}_x G$ and $\sigma_x^2 = \bar{n}_x G^2 F$, which shows the dependence of these parameters (i.e., μ_x and σ_x^2) and (i.e., G and F) on each other. At the same time, G denotes the internal current gain of APD, and k_{eff} denotes the ionization ratio and

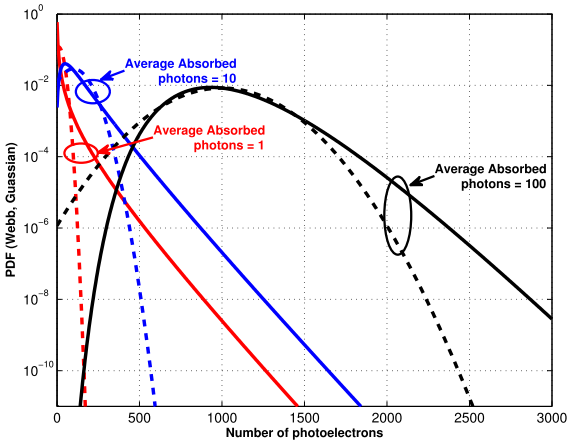

FIGURE 5. Probability density function of Webb and Gaussian Models.

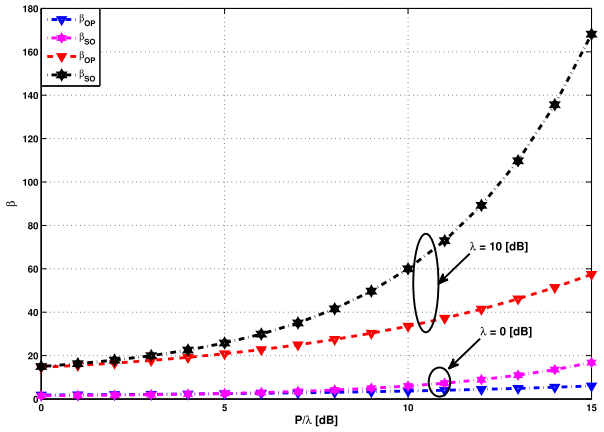

FIGURE 6. Detection threshold for given values of λ.

quantum efficiency. The relationship of these parameters is simplified as: $\mu_0 \approx \lambda G$, $\mu_1 \approx (\lambda + Ph)G$, $\sigma_0^2 \approx \lambda G^2 F$, $\sigma_1^2 \approx (\lambda + Ph)G^2 F$ [29]. In Fig. 5, we are considering the InGaAs APD with $G = 10$, $k_{eff} = 0.45$, $F = 5.5$ [30], we simulate the density functions for the Webb and IDGN model, which shows the agreement between the Webb and IDGN model near the distribution peaks.

IV. ERROR ANALYSIS

In the proposed work, the error analysis is done by exploiting the maximum likelihood approach (i.e., soft decision decoding) and machine learning.

A. MAXIMUM LIKELIHHOD APPROACH

The log-likelihood ratios (LLR) for the optical channel assuming the IDGN model is derived as,

$$\Lambda = \log\left(\frac{p(x=0|y,h)}{p(x=1|y,h)}\right) \tag{18}$$

where $p(x=1|y,h)$ denotes the probability of transmitting $x=1$ given that the received symbol y over a link fading and $p(x=0|y,h)$ denotes the probability of transmitting $x=0$ given the received symbol y over a link fading and. Using Bayes rule with the assumption of equi-likely transmitted bits, (18) is replaced by,

$$\Lambda = \log\left(\frac{p(y|x=0,h)}{p(y|x=1,h)}\right) \tag{19}$$

For the un-equi-likely input bits (i.e., $p(x) \neq 0.5$), we can re-write (19) as,

$$\Lambda = \log\frac{p(y|x=0,h)}{p(y|x=1,h)} + L(x) \tag{20}$$

where $L(x) = \log\left(\frac{p(x=0)}{p(x=1)}\right)$. The LLR mappings evaluate the BER, assuming the soft decision decoding. For the IDGN model, channel transition probabilities of bit "0" and "1", i.e., $p(y|x=0) \sim \mathcal{N}(\mu_0, \sigma_0^2)$ and $p(y|x=1) \sim \mathcal{N}(\mu_1, \sigma_1^2)$ are given by,

$$p(y|x=0) = \frac{1}{\sqrt{2\pi\sigma_0^2}}\exp\left(-\frac{(y-\mu_0)^2}{2\sigma_0^2}\right) \tag{21}$$

$$p(y|x=1) = \frac{1}{\sqrt{2\pi\sigma_1^2}}\exp\left(-\frac{(y-\mu_1)^2}{2\sigma_1^2}\right) \tag{22}$$

Using (21) and (22) in (19), the LLR mappings assuming the IDGN (Λ) and equi-likely transmitted bits with no scintillation and atmospheric attenuation,

$$\Lambda = \frac{1}{2}\log\left(1+\frac{P}{\lambda}\right) + \frac{1}{2G^2F\lambda(1+\frac{\lambda}{P})} \times \left[(G\lambda - y)(G\lambda + y) + G^2\lambda P\right] \tag{23}$$

Similarly, we derived LLR mappings considering the scintillation and atmospheric attenuation case as,

$$\Lambda = \frac{1}{2}\log\left(1+\frac{Ph}{\lambda}\right) + \frac{1}{2G^2F\lambda(1+\frac{\lambda}{Ph})} \times \left[(G\lambda - y)(G\lambda + y) + G^2\lambda Ph\right] \tag{24}$$

To evaluate the optimum optical signal detection threshold, the BER is minimized, and after further analysis, as is done in [4], the optimum β can be derived assuming the optimum and sub-optimum system,

$$\beta_{OP} = \sqrt{\lambda\left(1+\frac{\lambda}{Ph}\right)\left(P + \log\left(1+\frac{\lambda}{Ph}\right)\right)} \tag{25}$$

whereas, the $\beta_{SO} = \lambda + 0.5P$ for the sub-optimum system. The detection threshold results assume the optimum/sub-optimum system over a given value of $\lambda \in 0, 10$dB are shown in Fig. 6 and Fig. 7. It is evident from the simulation results that the changes in slope in the case of optimum and sub-optimum are SNR dependent. It changes fast for greater background irradiance and slowly for the small value.

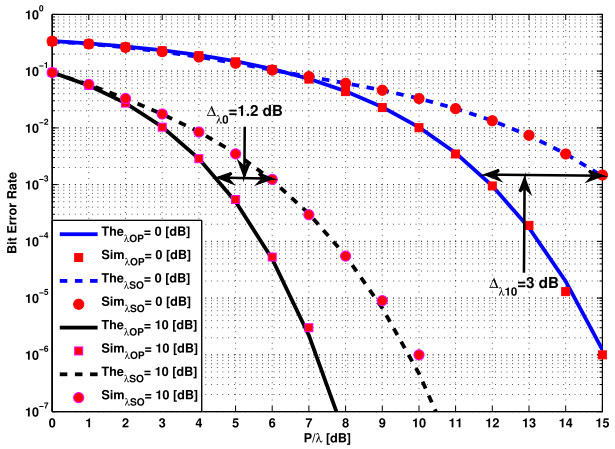

FIGURE 7. BER for $\sigma_I^2 = 0$ for varying λ.

B. MACHINE LEARNING APPROACH

Traditional algorithmic signal processing models involve solving numerical optimization, typically requiring longer converge iterations. Incorporating domain knowledge into the ML architectures could potentially expedite the training process and convergence and mainly improves the performance of the model. Techniques such as deep unfolding algorithms [48], and other hybrid models [49], [50] are gaining traction. Future communication and tracking systems will involve these deployments, slowly leading into the zone of federated learning [51], where devices make autonomous decisions while also interacting with other devices [52]. Furthermore, this improves the energy efficiency and longevity of the devices.

Neural networks generally approximate other functions by selecting the parameters to minimize the approximation error. In particular, fully-connected feed-forward networks can compare any continuous function arbitrarily well by utilizing a large but finite number of parameters. This can describe many real-world tasks, e.g. classification of objects on an image [53], transcription of a spoken sentence [54] or translation of a written sequence [55]. The approximation power of deep neural networks is the reason for their current success in various applications. ML-based solutions are increasingly being applied to solve complex signal processing tasks such as massive Multiple-Input Multiple-Output (MIMO) channel estimation and detection [56], beamforming, forward error correction (FEC) decoding [57], solving partial differential equations [58]. We envision that model-driven approaches might significantly influence future 6G networks with immense performance gains and ease of implementation. We can use ML approaches as an alternative to the standard engineering design when there is justification for its suitability, scalability and other advantages [59].

More recently, researchers have considered using an unsupervised learning framework called autoencoders for the joint design of coding and modulation schemes to remedy the channel impairments [60], [61]. Mostly autoencoders are applied to find a low-dimensional representation of the input and reconstruction implementation at the output with minimal error [62], [63].

The subscript θ in Fig. 4 denotes the functions with parameters adapted and learned to obtain a goal, e.g., minimizing the BER. We use the term autoencoders throughout this article. An autoencoder is a neural network architecture trained to replicate its input to its output [64], [65]. This is done in two stages as shown in Fig. 4 an encoder (i.e., mapping and encoding), which compresses its input to a lower dimension vector and a decoder (i.e., de-mapping and decoding) that seeks to replicate the original input from this lower dimensional non-linear manifold. Autoencoders are symmetrical in that the encoding layer is mimicked in the decoding layer as an inverted version of the encoding layer. They are typically used in non-linear dimensionality reduction, data denoising and compression.

An autoencoder is a composition of two parametric functions, an encoder f_{θ_T} and a decoder h_{θ_R}, to reproduce the input vector at the output. The parameter $\theta = \theta_T, \theta_R$ holds all trainable variables. The transmitter has to learn a meaningful representation of the input vector, which, when given to the decoder, holds enough information to replicate the input vector. To this end, the transmitter learns a higher-order constellation where the symbols align themselves in an optimal constellation geometry.

The receiver learns decision boundaries between the impaired symbols performing like a maximum likelihood detector for the received signals. The expectation is taken over each training batch. Since each message only has an individual non-zero value, the total N summation needs a single evaluation. The overall average of the cross-entropy of all samples is computed, and an estimate of the gradient concerning the model's parameters is done. The following steps are adopted to train the auto-encoder.

- **Batch Size**: batch size selection plays a vital role in decoder convergence and performance. The larger size results in slower convergence but optimum performance, and vice versa.
- **Training SNR**: SNR training with low and high values provides a better activity in the form of large to low error bits. Therefore, setting SNR such that the auto-encoder can have both the decoded blocks error and error-free.
- **Activation Function**: Adam optimizer [65] trains the network. It is suggested to start the training process with a smaller training batch size and increase it after the initial convergence to have the best trade-off between convergence speed, computation time and performance.

The ML model outperforms conventional techniques, such as the hard detection (HD) and soft detection (SD) model. The reviewers are quite correct in their argument about the better performance of machine learning, which is only possible if the model is trained well. The ML approach's training requires a large time and more computation. So there is a trade-off between the performance and the computational

TABLE 2. Simulation setup parameters (InGaAs-APD).

Parameters	Value	Parameters	Value
APD Gain (G)	10	Noise Factor	5.5
Wavelength	1550nm	Ionization ratio	0.45
λ	0, 10 [dB]	η	1
σ_I^2	0.5	Noise Temperature	300

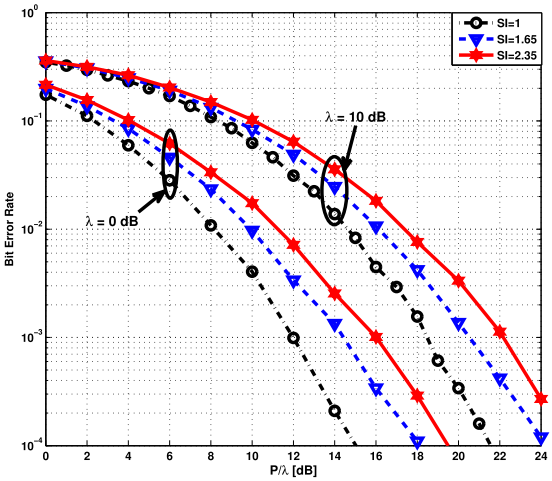

FIGURE 8. Bit error rate over varying scintillation and background irradiance.

complexity of all three approaches (hard decision (HD), soft decision (SD) and ML).

V. RESULTS AND DISCUSSION

A simulation setup parameters are given in Table 2, and bit error rate evaluation was performed for varying the values of scintillation and background irradiance. Simulation results for varying scintillation and background irradiance are shown in Fig. 8. Figure 8 is evaluated for $\sigma_I^2 = 1, 1.65, 2.35$ over a background irradiance of 0dB and 10dB. It shows that the smaller the values of σ_I^2 and λ, the better the bit error rate, which is obvious.

Further evaluation is performed for the hard decision, soft decision and machine learning, assuming a moderate weather conditions. From the simulation results, it is well observed that we are getting a desirable gain using the machine learning approach. Table 3 compares the performance gains for each technique under different configurations (cloudy, moderate and dense fog). It is noticed from Fig. 9 that for a given value of $\lambda = 0$ [dB], the ML approach gives 5[dB] and 2[dB] performance gains as compared to the hard and soft decision approach, respectively. Similarly, for a given value of $\lambda = 10$ [dB], the ML approach shows 4[dB] and 1[dB] performance gains as compared to the hard and soft decision approach, respectively.

It is noticed from the Table 3 that the ML approach outperforms the other conventional approaches, such as HD and SD. There is a trade-off to getting such performance; the trade-off is the training model for the ML approach and the computational complexity. The ML approach needs large data

TABLE 3. Comparison of detection approaches.

σ_I^2=0.5, BER = 10^{-4} (Cloudy)			
λ= 0 [dB]		λ= 10 [dB]	
Hard decision	12 [dB]	Hard decision	20 [dB]
Soft decision	9 [dB]	Soft decision	16 [dB]
ML approach	7 [dB]	ML approach	15 [dB]
Performance Gain			
ML vs. HD	5 [dB]	ML vs. HD	5 [dB]
ML vs. SD	2 [dB]	ML vs. SD	1 [dB]
σ_I^2=1.0, BER = 10^{-4} (Moderate Fog)			
Hard decision	15 [dB]	Hard decision	21.75 [dB]
Soft decision	12.5 [dB]	Soft decision	18.25 [dB]
ML approach	11.5 [dB]	ML approach	17.50 [dB]
Performance Gain			
ML vs. HD	4.50 [dB]	ML vs. HD	4.25 [dB]
ML vs. SD	1 [dB]	ML vs. SD	0.75 [dB]
σ_I^2=2.0, BER = 10^{-4} (Dense Fog)			
Hard decision	20 [dB]	Hard decision	26 [dB]
Soft decision	18 [dB]	Soft decision	23.25 [dB]
ML approach	17.50 [dB]	ML approach	22.90 [B]
Performance Gain			
ML vs. HD	2 [dB]	ML vs. HD	3.10 [dB]
ML vs. SD	0.5 [dB]	ML vs. SD	0.35 [dB]

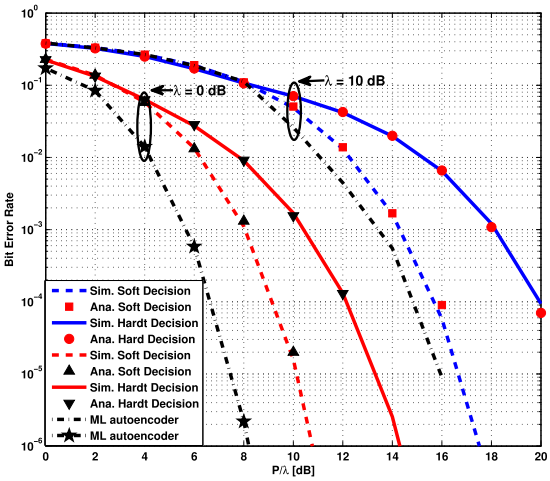

FIGURE 9. BER comparison of various detection techniques for σ_I^2=0.5.

TABLE 4. Experimental optical measuring setup parameters.

Parameters	Units	Values
Transmitter Power	mW	100
Antenna Aperture	mm	150
Wavelength	nm	1550
Coupling Efficiency		0.85
Link Distance	km	12
Transmit Antenna Beamwidth	mrad	0.5
FSO System Noise Temperature	K	1000

for training purposes, and ML's computational complexity is higher than the SD and HD approaches. The HD's performance is moderate compared to the SD and ML, but it is computationally in-extensive. The performance of SD is comparable to the ML approach, but it is computationally less expensive than the ML approach.

Experimental system evaluation is also done in the Institute for Telecommunication Research (ITR) laboratory, where a complete setup of the system exists. The experimental optical measuring setup parameters are given in Table 4. The

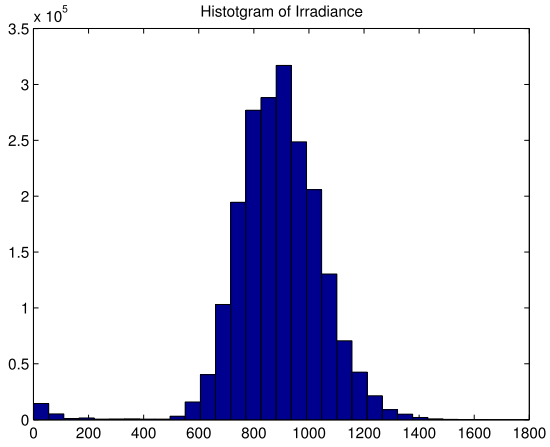

FIGURE 10. Histogram of channel response.

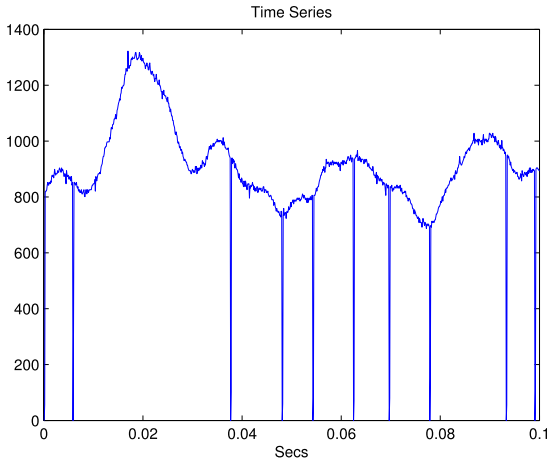

FIGURE 11. Channel impulse response.

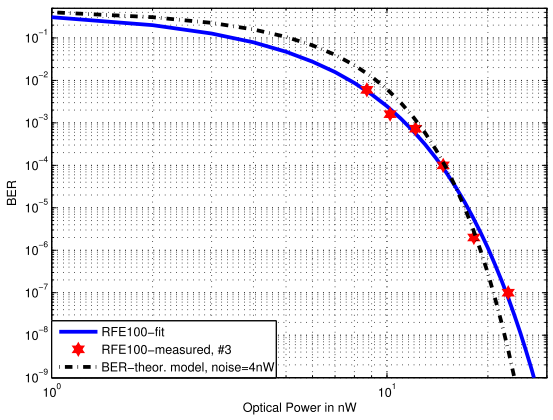

FIGURE 12. BER of channel with model fitting.

transmitter is set up at the ITR facility, and the receiver is installed 10Km away at Para Hills town. The channel model is retrieved, and the histogram and channel are plotted in Fig. 10 and 11, respectively. Then the performance curve of the measured channel is compared with the model fit using the ML approach and the theoretical curve shown in Fig. 12, which indicates that these values are better curve-fit models than the real receiver model.

VI. CONCLUSION

In the presented work, an error analysis of the FSO communication system is developed. Different detection approaches, such as hard, soft, and ML, have been analyzed under various weather and background irradiances. It is understood that the FSO channel gets distorted by factors such as scintillation, severe atmospheric weather scenarios, and pointing inaccuracies. Numerous techniques such as adaptive modulation, adaptive network topology, multiple access techniques, and optimization algorithms have been developed by many scientists to remedy such crucial problems of the optical channel. An analysis is developed to evaluate the system's performance. Among all these approaches (i.e., hard decision, soft decision and ML), the ML approach is new, providing good performance gains compared to the other approaches. The FSO system is more reliable and cost-effective. An experimental evaluation is also developed and presented in the proposed research work. An error analysis using the machine learning approach is developed and simulated. It shows that using the ML, error is reduced compared to the hard and soft decision approach. It indicates that ML performance is much better with reduced computational cost and improved BER performance.

VII. FUTURE RESEARCH DIRECTIONS AND ISSUES

To identify the research direction and discuss the open issues for the mitigation techniques in the vision of future sixth-generation (6G) wireless networks is still open. For satellite laser communications, opaque clouds can deteriorate or eliminate the FSO link from ground to satellite or satellite to ground, rendering the LOS communication useless. These intermittent issues can remain from a few seconds to several hours, depending on the geographical location and season. There are several practical transmission schemes for hybrid FSO/RF systems, such as single switching-based hybrid FSO/RF transmission schemes, hybrid FSO/RF systems with adaptive combining, and adaptive rate for hybrid FSO/RF systems. Our study provides a method for analyzing the impact of atmospheric and weather conditions. This analysis is not limited to single channels but can also be enhanced towards hybrid channels.

ACKNOWLEDGMENT

The authors would like to thank Prof. Bill Cowley and Khoa D. Nyugen from ITR, UniSA, SA, Australia, for their suggestion and useful discussion during the whole journey of this research work.

REFERENCES

[1] M. Singh, A. Atieh, A. Grover, and O. Barukab, "Performance analysis of 40 Gb/s free space optics transmission based on orbital angular momentum multiplexed beams," *Alexandria Eng. J.*, vol. 61, no. 7, pp. 5203–5212, Jul. 2022.

[2] Cisco. *10th Annual Cisco Visual Networking Index (VNI) Mobile Forecast Projects 70 Percent of Global Population Will be Mobile Users*. Accessed: Feb. 3, 2016. [Online]. Available: https://newsroom.cisco.com/press-releasecontent?articleId=1741352

[3] S. Bashir, M. H. Alsharif, I. Khan, M. A. Albreem, A. Sali, B. M. Ali, and W. Noh, "MIMO-terahertz in 6G nano-communications: Channel modeling and analysis," *Comput., Mater. Continua*, vol. 66, no. 1, pp. 263–274, 2020.

[4] D.-N. Nguyen, S. Zvanovec, and Z. Ghassemlooy, "Mitigation of dispersion and turbulence in a hybrid optical fibre and free-space optics link using electronic equalisation," *Optik*, vol. 196, Nov. 2019, Art. no. 163154.

[5] H. AlQuwaiee, I. S. Ansari, and M.-S. Alouini, "On the maximum and minimum of double generalized gamma variates with applications to the performance of free-space optical communication systems," *IEEE Trans. Veh. Technol.*, vol. 65, no. 11, pp. 8822–8831, Nov. 2016.

[6] R. Chowdhury, "Design and performance analysis of spectral-efficient hybrid CPDM-CO-OFDM FSO communication system under diverse weather conditions," *J. Opt. Commun.*, vol. 2021, Aug. 2021, Art. no. 000010151520210113, doi: 10.1515/joc-2021-0113.

[7] S. Bhatia and M. Singh, "Performance analysis in free space optical communication system using aperture averaging," in *Proc. 2nd Int. Conf. Comput. Commun. Technol.*, New Delhi, India, 2016, pp. 319–327.

[8] H. Henniger and O. Wilfert, "An introduction to free-space optical communications," *Radioengineering*, vol. 19, no. 2, pp. 203–212, 2010.

[9] L. S. A. Jabeena, T. Jayabarathi, and R. Aggarwal, "Review on optimization of wireless optical communication system," *Trends Opto-Electro Opt. Commun.*, vol. 4, pp. 9–19, Apr. 2019.

[10] A. Gupta, P. Anand, R. Khajuria, S. Bhagat, and R. K. Jha, "Survey of free space optical communication network channel over optical fiber cable communication," *Int. J. Comput. Appl.*, vol. 105, no. 105, pp. 32–36, 2014.

[11] D. Dhawan, "Reducing the effect of scintillation in FSO system using coherent based homodyne detection," *Optik*, vol. 171, no. 1, pp. 6–20, Oct. 2018.

[12] A. Ahmed, S. Gupta, Y. Luthra, K. Gupta, and S. Kaur, "Analysing the effect of scintillation on free space optics using different scintillation models," in *Proc. 6th Int. Conf. Signal Process. Integr. Netw. (SPIN)*, Noida, India, Mar. 2019, pp. 799–804.

[13] E. Erdogan, N. Kabaoglu, I. Altunbas, and H. Yanikomeroglu, "On the error probability of cognitive RF-FSO relay networks over Rayleigh/EW fading channels with primary-secondary interference," *IEEE Photon. J.*, vol. 12, no. 1, pp. 1–13, Feb. 2020.

[14] V. Alexander, S. Hg, and D. Varoutas, "Weather effects on FSO network connectivity," *J. Opt. Commun. Netw.*, vol. 4, pp. 734–740, Jan. 2012.

[15] M. Ijaz, Z. Ghassemlooy, J. Perez, V. Brazda, and O. Fiser, "Enhancing the atmospheric visibility and fog attenuation using a controlled FSO channel," *IEEE Photon. Technol. Lett.*, vol. 25, no. 13, pp. 1262–1265, May 17, 2013.

[16] T. Fahey, M. Islam, A. Gardi, and R. Sabatini, "Laser beam atmospheric propagation modelling for aerospace LiDAR applications," *Atmosphere*, vol. 12, no. 7, p. 918, Jul. 2021.

[17] L. C. Andrews, R. L. Phillips, and C. Y. Hopen, *Laser Beam Scintillation With Applications*. Bellingham, WA, USA: SPIE Press, 2001.

[18] A. M. Aly, H. A. Fayed, N. E. Ismail, and M. H. Aly, "Plane wave scintillation index in slant path atmospheric turbulence: Closed form expressions for uplink and downlink," *Opt. Quantum Electron.*, vol. 52, no. 7, pp. 1–14, Jul. 2020.

[19] O. O. Kolawole, T. J. O. Afullo, and M. Mosalaosi, "Terrestrial free space optical communication systems availability based on meteorological visibility data for South Africa," *SAIEE Afr. Res. J.*, vol. 113, no. 1, pp. 20–36, Mar. 2022.

[20] Z. Xu, G. Xu, and Z. Zheng, "BER and channel capacity performance of an FSO communication system over atmospheric turbulence with different types of noise," *Sensors*, vol. 21, no. 10, pp. 34–54, 2021.

[21] H. D. Le, T. V. Nguyen, and A. T. Pham, "Cloud attenuation statistical model for satellite-based FSO communications," *IEEE Antennas Wireless Propag. Lett.*, vol. 20, no. 5, pp. 643–647, Feb. 2021.

[22] B. Lacaze, "Gaps of free-space optics beams with the Beer–Lambert law," *Appl. Opt.*, vol. 48, no. 14, pp. 2702–2706, May 2009.

[23] M. Ijaz, Z. Ghassemlooy, J. Pesek, O. Fiser, H. L. Minh, and E. Bentley, "Modeling of fog and smoke attenuation in free space optical communications link under controlled laboratory conditions," *J. Lightw. Technol.*, vol. 31, no. 11, pp. 1720–1726, Jun. 1, 2013.

[24] N. Kumar and H. Sohal, "Impact of various weather condition on the performance of free space optical communication system," *J. Opt. Commun.*, vol. 35, no. 1, pp. 45–49, Jan. 2014.

[25] H. D. Le and A. T. Pham, "Link-layer retransmission-based error-control protocols in FSO communications: A survey," *IEEE Commun. Surveys Tuts.*, vol. 24, no. 3, pp. 1602–1633, 3rd Quart., 2022.

[26] P. P. Webb, R. J. McIntyre, and J. Conradi, "Properties of avalanche photodiodes," *RCA Rev.*, vol. 35, no. 2, pp. 234–278, Jun. 1974.

[27] R. J. McIntyre, "The distribution of gains in uniformly multiplying avalanche photodiodes: Theory," *IEEE Trans. Electron Devices*, vol. ED-19, no. 6, pp. 703–713, Jun. 1972.

[28] P. Vishwakarma and J. Vijay, "Comparative analysis of free space optics and single mode fiber," *Int. J. Adv. Eng., Manage. Sci.*, vol. 2, no. 1, 2016, Art. no. 239367.

[29] M. N. Khan and W. G. Cowley, "Signal dependent Gaussian noise model for FSO communications," in *Proc. Austral. Commun. Theory Workshop*, Jan. 2011, pp. 142–147.

[30] M. N. Khan, S. O. Gilani, M. Jamil, A. Rafay, Q. Awais, B. A. Khawaja, M. Uzair, and A. W. Malik, "Maximizing throughput of hybrid FSO-RF communication system: An algorithm," *IEEE Access*, vol. 6, pp. 30039–30048, 2018.

[31] A. C. Boucouvalas, "Challenges in optical wireless communications," *Opt. Photon. news*, vol. 16, no. 9, pp. 36–39, Sep. 2005.

[32] A. Mansour, R. Mesleh, and M. Abaza, "New challenges in wireless and free space optical communications," *Opt. Lasers Eng.*, vol. 89, pp. 95–108, Feb. 2017.

[33] S. Sharma, A. S. Madhukumar, and R. Swaminathan, "Effect of pointing errors on the performance of hybrid FSO/RF networks," *IEEE Access*, vol. 7, pp. 131418–131434, 2019.

[34] M. N. Khan, M. Jail, and M. Hussain, "Adaptation of hybrid FSO/RF communication system using puncturing technique," *Radioengineering*, vol. 25, no. 4, pp. 12–19, 2016.

[35] M. N. Khan and M. Jamil, "Adaptive hybrid free space optical/radio frequency communication system," *Telecommun. Syst.*, vol. 65, no. 1, pp. 117–126, May 2017.

[36] T. V. Nguyen, H. D. Le, and A. T. Pham, "On the design of RIS-UAV relay-assisted hybrid FSO/RF satellite-aerial-ground integrated network," *IEEE Trans. Aerosp. Electron. Syst.*, early access, Jul. 8, 2022, doi: 10.1109/TAES.2022.3189334.

[37] T. V. Nguyen, T. V. Pham, N. T. Dang, and A. T. Pham, "Performance of generalized QAM/FSO systems with pointing misalignment and phase error over atmospheric turbulence channels," *IEEE Access*, vol. 8, pp. 203631–203644, 2020.

[38] E. Erdogan, I. Altunbas, G. K. Kurt, M. Bellemare, G. Lamontagne, and H. Yanikomeroglu, "Site diversity in downlink optical satellite networks through ground station selection," *IEEE Access*, vol. 9, pp. 31179–31190, 2021.

[39] M. Naghshvarianjahromi and K. Shiva, "Free space ground to satellite optical communications using Kramers–Kronig transceiver in the presence of atmospheric turbulence," *Sensors*, vol. 22, no. 9, p. 3534, 2022.

[40] A. S. Alatawi, A. A. Youssef, M. Abaza, M. A. Uddin, and A. Mansour, "Effects of atmospheric turbulence on optical wireless communication in NEOM smart city," *Photonics*, vol. 9, no. 4, p. 262, Apr. 2022.

[41] H. Singh and N. Mittal, "Analyzing the impact of fog and atmospheric turbulence on the deployment of free-space optical communication links in India," *Arabian J. Sci. Eng.*, vol. 47, pp. 2691–2710, Jan. 2022.

[42] O. O. Erunkulu, A. M. Zungeru, C. K. Lebekwe, M. Mosalaosi, and J. M. Chuma, "5G mobile communication applications: A survey and comparison of use cases," *IEEE Access*, vol. 9, pp. 97251–97295, 2021.

[43] P. K. Singya, P. Shaik, N. Kumar, V. Bhatia, and M.-S. Alouini, "A survey on higher-order QAM constellations: Technical challenges, recent advances, and future trends," *IEEE Open J. Commun. Soc.*, vol. 2, pp. 617–655, 2021.

[44] M. N. Khan, "Importance of noise models in FSO communications," *EURASIP J. Wireless Commun. Netw.*, vol. 2014, no. 1, pp. 1–10, Dec. 2014.

[45] S. Arnon, J. Barry, G. Karagiannidis, R. Schober, and M. Uysal, *Advanced Optical Wireless Communication Systems*. Cambridge, U.K.: Cambridge Univ. Press, 2012.

[46] R. Samy, H. C. Yang, T. Rakia, and M. S. Alouini, "Performance analysis of hybrid SAG-FSO/RF satellite communication system," *TechRxiv*, doi: 10.36227/techrxiv.19623849.v1.

[47] S. M. Yasir, N. Abas, S. Rauf, N. R. Chaudhry, and M. S. Saleem, "Investigation of optimum FSO communication link using different modulation techniques under fog conditions," *Heliyon*, vol. 8, no. 12, Dec. 2022, Art. no. e12516.
[48] A. Balatsoukas-Stimming and C. Studer, "Deep unfolding for communications systems: A survey and some new directions," in *Proc. IEEE Int. Workshop Signal Process. Syst. (SiPS)*, Nanjing, China, Oct. 2019, pp. 266–271.
[49] M. L. Weiss, R. C. Paffenroth, and J. R. Uzarski, "The autoencoder-Kalman filter: Theory and practice," in *Proc. 53rd Asilomar Conf. Signals, Syst., Comput.*, Pacific Grove, CA, USA, Nov. 2019, pp. 2176–2179.
[50] M. Weiss, R. C. Paffenroth, J. R. Whitehill, and J. R. Uzarski, "Deep learning with domain randomization for optimal filtering," in *Proc. 18th IEEE Int. Conf. Mach. Learn. Appl. (ICMLA)*, Boca Raton, FL, USA, Dec. 2019, pp. 1779–1786.
[51] Z. Qin, G. Ye Li, and H. Ye, "Federated learning and wireless communications," 2020, *arXiv:2005.05265*.
[52] T. Li, A. K. Sahu, A. Talwalkar, and V. Smith, "Federated learning: Challenges, methods, and future directions," *IEEE Signal Process. Mag.*, vol. 37, no. 3, pp. 50–60, May 2020.
[53] Y. LeCun, Y. Bengio, and G. Hinton, "Deep learning," *Nature*, vol. 521, no. 7553, p. 436, Feb. 2015.
[54] J. Schmidhuber, "Deep learning in neural networks: An overview," *Neural Netw.*, vol. 61, pp. 85–117, Jan. 2014.
[55] I. Goodfellow, Y. Bengio, and A. Courville, *Deep Learning*. Cambridge, MA, USA: MIT Press, 2016.
[56] F. A. Aoudia and J. Hoydis, "End-to-end learning of communications systems without a channel model," 2018, *arXiv:1804.02276*.
[57] H. Kim, Y. Jiang, S. Kannan, S. Oh, and P. Viswanath, "DeepCode: Feedback codes via deep learning," in *Proc. Adv. Neural Inf. Process. Syst.*, Montréal, QC, Canada, 2018, pp. 9458–9468.
[58] L. Ambrogioni, U. Güçlü, E. Maris, and M. van Gerven, "Estimating nonlinear dynamics with the ConvNet smoother," 2017, *arXiv:1702.05243*.
[59] S. Cammerer, F. A. Aoudia, S. Dörner, M. Stark, J. Hoydis, and S. T. Brink, "Trainable communication systems: Concepts and prototype," *IEEE Trans. Commun.*, vol. 68, no. 9, pp. 5489–5503, Sep. 2020, doi: 10.1109/TCOMM.2020.3002915.
[60] T. O'Shea and J. Hoydis, "An introduction to deep learning for the physical layer," *IEEE Trans. Cogn. Commun. Netw.*, vol. 3, no. 4, pp. 563–575, Dec. 2017, doi: 10.1109/TCCN.2017.2758370.
[61] S. Dörner, S. Cammerer, J. Hoydis, and S. T. Brink, "Deep learning based communication over the air," *IEEE J. Sel. Topics Signal Process.*, vol. 12, no. 1, pp. 132–143, Feb. 2018.
[62] P. Vincent, H. Larochelle, I. Lajoie, Y. Bengio, and P.-A. Manzagol, "Stacked denoising autoencoders: Learning useful representations in a deep network with a local denoising criterion," *J. Mach. Learn. Res.*, vol. 11, no. 12, pp. 3371–3408, Dec. 2010.
[63] T. J. Oshea, T. Roy, N. West, and B. C. Hilburn, "Physical layer communications system design over-the-air using adversarial networks," in *Proc. 26th Eur. Signal Process. Conf. (EUSIPCO)*, Rome, Italy, Sep. 2018, pp. 529–532.
[64] Y. Bengio, "Learning deep architectures for AI," *Found. Trends Mach. Learn.*, vol. 2, no. 1, pp. 1–27, 2009.
[65] D. P. Kingma and J. Ba, "Adam: A method for stochastic optimization," 2014, *arXiv:1412.6980*.

ALI A. ALTALBE received the M.Sc. degree in information technology from Flinders University, Australia, and the Ph.D. degree in information technology from The University of Queensland, Australia. He is currently working as an Assistant Professor with the Department of IT.

MUHAMMAD NASIR KHAN received the B.E. degree in electronic engineering from the Dawood University of Engineering and Technology, Karachi, Pakistan, in 2002, the two M.Sc. degrees (Hons.) in electrical engineering one from the University of Engineering and Technology, Lahore, Pakistan, and one from the Technical University of Delft, The Netherlands, in 2007 and 2009, respectively, and the Ph.D. degree in telecommunications from the Institute for Telecommunication Research, University of South Australia, Australia, in 2013. Currently, he is working as a Professor with the Electrical Engineering Department, The University of Lahore, Pakistan. His research interests include channel coding, detection theory, development of energy efficient algorithm for wireless sensor networks, signal processing for communication, machine learning, and optimization techniques.

MUHAMMAD TAHIR received the B.S. degree in computer engineering from Sir Syed University, the M.E. degree in computer system from NED University, and the Ph.D. degree in information science from the University of Roma Tor Vergata. He is currently an Associate Professor with the Sir Syed University of Engineering and Technology, Karachi. His research interests include IP switches/routing, IPv4 protocol, firewall, the IoT, VR/AR, block chain, cryptography, and wireless sensor networks.